Available online at www.sciencedirect.com

ScienceDirect

IFAC PapersOnline CONFERENCE PAPER ARCHIVE

IFAC PapersOnLine 56-2 (2023) 11778–11783

Model-plant mismatch detection for a plant under Model Predictive Control: A grinding mill circuit case study

Heinz K. Mittermaier * **Johan D. le Roux** *,1
Laurentz E. Olivier *,** **Ian K. Craig** *

* *Department of Electrical, Electronic, and Computer Engineering, University of Pretoria, Pretoria, South Africa.*
** *Analyte Control, Pretoria, South Africa.*

Abstract: This articles investigates two different techniques of identifying model-plant mismatch for a grinding mill circuit under model predictive control. A previous attempt at model-plant mismatch detection for a grinding mill, in the form of a partial cross correlation analysis, is used as a benchmark for model-plant mismatch detection and degraded sub-model isolation. This is followed by an investigation of the plant model ratio technique applied to the same system. The plant model ratio technique is able to isolate the sub-model containing a mismatch as well as detect the specific parameter in a first-order-plus-time-delay model responsible for the mismatch. A simulation study is used to quantify and compare the results between the two model-plant mismatch detection methodologies. The results indicate plant model ratio accurately and timeously detects mismatches in sub-models. This allows for system reidentification or controller adaption to ensure optimal process performance. The advantage above partial cross correlation is the parameter diagnosis within the degraded sub-model coupled with the mismatch direction.

Keywords:
Controller performance monitoring, grinding mill circuit, model predictive control, model-plant mismatch, process performance monitoring.

1. INTRODUCTION

One of the predominant factors of process control is that a change in process dynamics is unavoidable. These changes in dynamics can cause performance deterioration of model-based controllers over time and significantly reduce the performance benefit of model predictive controllers (MPC) (Qin and Badgwell, 2003; Mayne, 2014; Schwenzer et al., 2021). This is one of the reasons why decoupled classical proportional-integral-derivative controllers are often favoured above advanced process control (APC) methods for multiple-input multiple-output (MIMO) plants, especially when applied to grinding mill circuits (Wei and Craig, 2009; Hodouin, 2011; Olivier and Craig, 2017).

Direct and indirect methods of controller performance monitoring (CPM) in the form of model-plant mismatch (MPM) detection and isolation have been identified and developed to the point where MPM can be identified in an on-line fashion, with minimal process disruption (Wu and Du, 2022).

The principal categories for the indirect methods are statistical-based techniques and sensitivity function-based techniques. Badwe et al. (2009) proposed a partial correlation analysis on which most of the statistical-based methodologies are based. The proposed partial correlation analysis is between the model residuals and the manipulated variables (MVs). Li et al. (2020) proposed a correlation analysis between the inputs and the disturbances of the process being controlled. In addition to partial correlation, other statistical-based techniques include the plant model ratio (PMR) (Selvanathan and Tangirala, 2010), the variance ratio-based model evaluation index (Ling et al., 2017) and an autocovariance-based method to identify process parameter values (Xu et al., 2020). Sensitivity function-based techniques include a dual validation algorithm, based on the two-model divergence method (Jiang et al., 2009), the estimation of Markov parameters using an integrated moving window and subspace approach (Yin et al., 2014) and an improved PMR with minimal excitation (Kaw et al., 2014).

The predominant direct method of MPM detection was proposed by Tsai et al. (2015). This method is based on using small sinusoidal test signals to estimate the process frequency responses. The MPM is detected using this frequency response, followed by an isolation of the degraded model of the plant.

The contribution of this paper is the application of PMR, extended for the use on MIMO systems (Yerramilli and Tangirala, 2016), to a run-of-mine (ROM) ore grinding mill circuit under MPC control. The grinding mill circuit is represented using a linear time invariant (LTI) approximation of a non-linear model of the milling circuit (Coetzee

⋆ This work is based on the research supported in part by the National Research Foundation of South Africa (Grant Numbers: 137769)
[1] Corresponding author, E-mail: derik.leroux@up.ac.za

10.1016/j.ifacol.2023.10.566

et al., 2010). Applicable model uncertainties for the ROM ore milling circuit (Craig and MacLeod, 1995) are used to introduce MPM into the simulation. The PMR results are compared to the MPM results of Olivier and Craig (2011) where the sub-model of the grinding mill circuit containing MPM could be isolated. PMR can refine the results by isolating the degraded sub-model as well as diagnosing the specific sub-model parameter(s) that contain the mismatch.

2. MODEL PREDICTIVE CONTROL

The aim of a discrete-time linear MPC is expressed as

$$\mathbf{u} = \arg\min J\left(\mathbf{u}^{N_C}\right) \tag{1a}$$

given that,

$$J\left(\mathbf{u}^{N_C}\right) = \sum_{j=1}^{N_P} \left\| \mathbf{e}^{y}_{k+j} \right\|_{\mathbf{Q}} + \sum_{j=0}^{N_C-1} \left\| \Delta \mathbf{u}_{k+j} \right\|_{\mathbf{R}} \tag{1b}$$

subject to

$$\begin{aligned} &\mathbf{x}_{k+j} = \mathbf{A}\left(\mathbf{x}_{k+j-1}\right) + \mathbf{B}\left(\mathbf{u}_{k+j-1}\right) \quad \forall j = 1, N_p \\ &\mathbf{y}_{k+j} = \mathbf{C}\left(\mathbf{x}_{k+j-1}\right) + \mathbf{D}\left(\mathbf{u}_{k+j-1}\right) \quad \forall j = 1, N_p \\ &\underline{\mathbf{u}} \le \mathbf{u}_{k+j} \le \overline{\mathbf{u}} \quad \forall j = 0, N_C - 1, \\ &\Delta\underline{\mathbf{u}} \le \Delta\mathbf{u}_{k+j} \le \Delta\overline{\mathbf{u}} \quad \forall j = 0, N_C - 1. \end{aligned} \tag{1c}$$

The objective function minimizes the difference between the predicted plant output and the current set-point of the plant, defined as $\mathbf{e}^{y}_{k+j} \equiv \mathbf{y}_{k+j} - \mathbf{y}^{\mathbf{r}}_{k+j}$, over the length of the prediction horizon, N_P. The objective function minimizes the rate of change of the control actions defined as $\Delta\mathbf{u}_{k+j} = \mathbf{u}_{k+j} - \mathbf{u}_k$ over the control horizon, N_C. The terms in the objective function are assigned relative weights in the form of positive definite matrices ($\mathbf{Q}$ and $\mathbf{R}$) to force desirable behaviour on the plant using the controller. $\mathbf{Q}$ is a positive definite matrix and $\mathbf{R}$ is a positive semi-definite matrix. The solution to the optimization is: $\mathbf{u}^{N_C} = (\, \mathbf{u}_k \;\; \mathbf{u}_{k+1} \;\cdots\; \mathbf{u}_{k+N_C-1} \,)$. For each MPC interval, $\mathbf{u}_k$ is applied to the plant and the optimization is repeated (Qin and Badgwell, 2003).

3. MILLING CIRCUIT MODEL

Fig. 1 depicts the grinding mill circuit used to test the MPM methodologies. The MIMO system consist of three MVs, mill feed ore (u_{MFO}), mill inlet water (u_{MIW}) and sump feed water (u_{SFW}) along with three controlled variables (CV), mill load (y_{J_T}), sump fill (y_{SLEV}) and particle size (y_{PSE}). A hydrocyclone is used in a closed circuit with the mill to separate the product from the out-of-specification material. The underflow of the cyclone, combined with the feed ore, water and steel balls accounts for the feed to the mill. It should be noted that the mill inlet water is manipulated as a ratio of the mill feed ore and the added steel balls are considered as constant. The mill discharges the ground slurry into a sump through an end-discharge grate. The ground slurry is diluted with water before being pumped to the cyclone for classification. The overflow of the hydrocyclone is the product of the milling circuit (Coetzee et al., 2010; le Roux and Craig, 2019).

The linear time invariant (LTI) model representation of a grinding mill circuit from Olivier and Craig (2011) is used in this study. System identification was used used to obtain an LTI representation of the non-linear grinding mill circuit simulation model of Coetzee et al. (2010). Step test data was created for 60 hours at the operating conditions as shown in Table 1. The following 9 models were obtained,

Table 1. Grinding mill circuit variable constraints and operating points (OP).

Variable	Min	Max	OP	Unit	Description
u_{MIW}	0	100	33.3	m^3/h	Flow-rate of water to the mill
u_{MFO}	0	200	100	t/h	Flow-rate of solids to the mill
u_{SFW}	0	400	267	m^3/h	Flow-rate of water to the sump
y_{PSE}	60	90	80	%	Product particle size $< 75\mu m$
y_{J_T}	30	50	45	%	Total charge of the mill
y_{SLEV}	2	9.5	5	m^3	Level of the sump

$$\begin{bmatrix} \Delta y_{PSE} \\ \Delta y_{J_T} \\ \Delta y_{SLEV} \end{bmatrix} = \begin{bmatrix} g_{11} & g_{12} & g_{13} \\ g_{21} & g_{22} & g_{23} \\ g_{31} & g_{32} & g_{33} \end{bmatrix} \begin{bmatrix} \Delta u_{CFF} \\ \Delta u_{MFO} \\ \Delta u_{SFW} \end{bmatrix} \tag{2a}$$

where g_{1j} is in the form,

$$g_{1j} = \frac{k_{1j}}{s + \alpha_{1j}} e^{-\theta_{1j}} \tag{2b}$$

with $k_{11} = -2.4 \times 10^{-4}$, $k_{12} = -5.99 \times 10^{-4}$, $k_{13} = 1.45 \times 10^{-3}$; $\alpha_{11} = 0.5882$, $\alpha_{12} = 1.353$, $\alpha_{13} = 2.216$; and $\theta_{11} = 0.011$, $\theta_{12} = 0.0639$, $\theta_{13} = 0.011$. The remaining transfer functions are in the form,

$$g_{ij} = \frac{k_{ij}}{s + 10^{-6}} \tag{2c}$$

with $k_{21} = 7.15 \times 10^{-4}$, $k_{22} = 7.22 \times 10^{-3}$, $k_{23} = -1.39 \times 10^{-3}$, $k_{31} = -0.60$, $k_{32} = 0.0097$ and $k_{33} = 0.774$. The time units for the model is in hours. Both the simulation environment and the controller will use the linearized model in (2).

4. PARTIAL CORRELATION ANALYSES

Badwe et al. (2009) proposed using the partial correlation analyses between the model residuals and the MVs to detect and isolate MPM in MPC applications. A superficial correlation may exist between different MVs based on the optimisation of the MPC algorithm. The partial

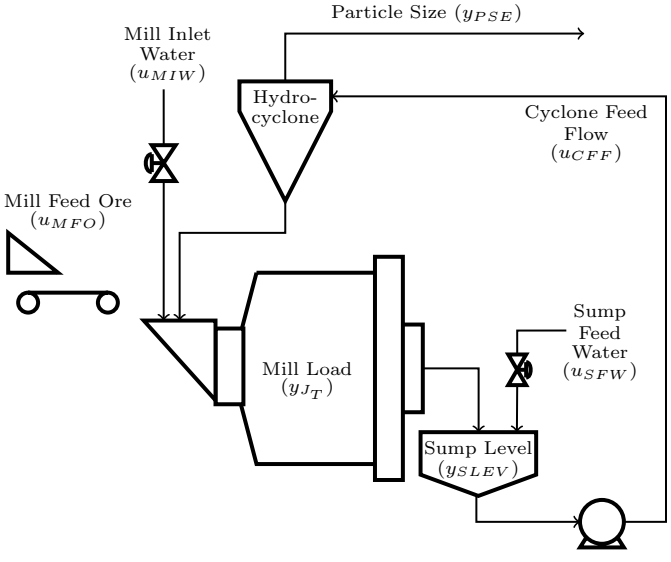

Fig. 1. Single-stage closed grinding mill circuit.

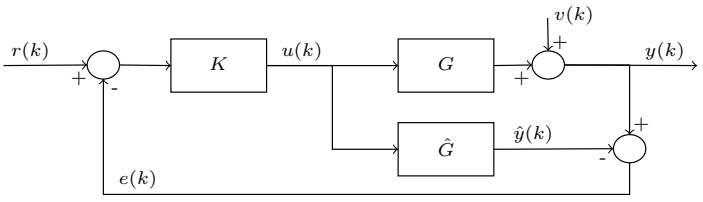

Fig. 2. Closed-loop IMC structure

correlation approach would detect hidden correlations and inhibit the detection of spurious correlations.

From the internal model control (IMC) structure in Fig. 2, the residuals between the plant (G) and the model ($\hat{G}$) are,

$$e(k) = y(k) - \hat{y}(k) = \Delta G u(k) + v(k) \tag{3}$$

where $\Delta G = (G - \hat{G})$ is the MPM. Therefore, the amount of mismatch, ΔG, can be obtained using a correlation analysis between $e(k)$ and $u(k)$. The input sensitivities from the setpoint $r(k)$ to the output noise $v(k)$ can be obtained from Fig. 2 as,

$$u(k) = K[I + \Delta GK]^{-1} r(k) - K[I + \Delta GK]^{-1} v(k) \tag{4}$$

Since the sensitivity functions are used, the MPM analyses should be performed on a recorded dataset where sufficient setpoint excitation is present to ensure estimation accuracy of the uncorrelated components ϵ_{u_i} and ϵ_{e_j} (as defined below in (6) and (7)). To guarantee that the MV disturbances do not lead to the misidentification of MPM, disturbance free MVs ($\hat{u}^r(k)$) are required (Badwe et al., 2009).

For $\hat{u}^r(k)$, the component of each MV that is uncorrelated with all other MVs is computed. Each MV can be represented as,

$$\hat{u}_i^r(k) = G_{u_i} \tilde{u}^r(k) + \epsilon_{u_i}(k) \tag{5}$$

where G_{u_i} is a model identified between u_i^r and all other MVs. $\tilde{u}^r$ contains all MVs except for u_i (the i^{th} MV), while ϵ_{u_i} is the component of u_i that is uncorrelated with all other MVs. Therefore, ϵ_{u_i} can be written as,

$$\hat{\epsilon}_{u_i}(k) = \hat{u}^r(k)_i - G_{u_i} \tilde{u}^r(k) \tag{6}$$

The same methodology is used to calculate the component of each residual, which is uncorrelated with all other MVs, except u_i,

$$\hat{\epsilon}_{e_j}(k) = e_j(k) - G_{e_j} \tilde{u}^r(k). \tag{7}$$

where j denotes the uncorrelated CV and G_{e_j} is the model identified between residuals e_j and all other MVs except u_i. Using (6) and (7), a non-zero correlation between $\hat{\epsilon}_{u_i}$ and $\hat{\epsilon}_{e_j}$ will indicate MPM in the $u_i - y_j$ channel (Badwe et al., 2009; Olivier and Craig, 2011).

5. PLANT MODEL RATIO

The aim of PMR, as developed for single-input single-output (SISO) systems, is to identify, isolate and diagnose the MPM as either a gain mismatch, a delay mismatch, a dynamic mismatch, or a combination of the three different types of mismatches (Selvanathan and Tangirala, 2010). Owing to modelling uncertainties and the lack of accurate process knowledge, the conventional description for MPM, ΔG, is seldom zero. Model parameter degradation, imprecise parameter estimation and non-linearities can cause

Table 2. MPM analysis using PMR

	Assessment Procedure	**Diagnosis of MPM**
Step 1	$M(\omega)\|_{\omega=0} \neq 1$	$K_G \neq K_{\hat{G}}$ else $K_G = K_{\hat{G}}$
Step 2	$M(\omega)$ has a zero initial slope (flatness test)	if flat, $\tau_G = \tau_{\hat{G}}$, else $\tau_G \neq \tau_{\hat{G}}$
Step 3	Linearity check of $\Delta P(\omega)$	if linear: $D_G \neq D_{\hat{G}}$, else $D_G = D_{\hat{G}}$

MPM, leading to a nonzero ΔG, and therefore for SISO systems the PMR is defined as the ratio of the frequency response function of the plant ($G(e^{j\omega})$) to the frequency response function of the model ($\hat{G}(e^{j\omega})$),

$$G_{PMR}(e^{j\omega}) = \frac{G(e^{j\omega})}{\hat{G}(e^{j\omega})} = M(\omega) e^{j\Delta P(\omega)} \tag{8}$$

As discussed by Selvanathan and Tangirala (2010), the gain mismatch information is contained in $M(\omega)$, the phase mismatch information is contained in $\Delta P(\omega)$ and the dynamic mismatch influences both magnitude and phase responses of PMR in (8). This property of the PMR leads to the systematic method of diagnosing the type of MPM, seen in Table 2, where K, τ and D represents the gain, dynamic and delay characteristic, respectively. Furthermore, the PMR also defines the direction of the MPM, identifying whether the plant parameter is greater or smaller than the corresponding model parameter. An additional advantage of using a frequency-domain based technique, as opposed to a time domain counterpart, is that an analysis can be performed over a specific band of frequencies, allowing for an efficient handling of signals containing noise.

To mitigate the effects of noise, PMR can be estimated for a SISO system using the correlation between plant and model output and the set-point,

$$\Pi_G = \frac{\hat{\gamma}_{y,r}(\omega)}{\hat{\gamma}_{\hat{y},r}(\omega)} \tag{9}$$

where $\hat{\gamma}_{y,r}(\omega)$ is the estimated cross-spectral density (CSD) between the plant output $y(k)$ and the set-point $r(k)$ (Selvanathan and Tangirala, 2010).

5.1 PMR expanded to MIMO systems

For MIMO systems, from the IMC structure in Fig. 2, the plant output y_i can be expressed in terms of the model output $\hat{y}_i$,

$$\begin{aligned} y_i(\omega) &= \sum_{k=1}^{n} G_{ik}(\omega) u_k(\omega) + d_i(\omega) \\ &= \sum_{k=1}^{n} \Pi_{G,ik}(\omega) \hat{G}_{ik}(\omega) u_k(\omega) + d_i(\omega) \\ &= \sum_{k=1}^{n} \Pi_{G,ik}(\omega) \hat{y}_{ik}(\omega) + d_i(\omega) \end{aligned} \tag{10}$$

where $\hat{y}_{ik}$ is the k^{th} component, of the i^{th} model output ($\hat{y}_i$), corresponding to the k^{th} input u_k.

For an $n \times n$ MIMO system, the element-wise division between the plant and model transfer function matrices identifies the PMR matrix (Yerramilli and Tangirala, 2016),

$$\mathbf{\Pi_G}(\omega) = \begin{bmatrix} \frac{G_{11}(\omega)}{\hat{G}_{11}(\omega)} & \frac{G_{12}(\omega)}{\hat{G}_{12}(\omega)} & \cdots & \frac{G_{1n}(\omega)}{\hat{G}_{1n}(\omega)} \\ \vdots & \vdots & \ddots & \vdots \\ \frac{G_{n1}(\omega)}{\hat{G}_{n1}(\omega)} & \frac{G_{n2}(\omega)}{\hat{G}_{n2}(\omega)} & \cdots & \frac{G_{nn}(\omega)}{\hat{G}_{nn}(\omega)} \end{bmatrix} \tag{11}$$

By combining (10) and (11), the estimated PMR for uncorrelated MIMO systems will be,

$$\hat{\mathbf{\Pi}}_{\boldsymbol{G}}(\omega) = \frac{\hat{\gamma}_{y_i,\hat{y}_{ij}}(\omega)}{\hat{\gamma}_{\hat{y}_{ij},\hat{y}_{ij}}(\omega)} \tag{12}$$

where the i^{th} row of the PMR matrix in (11) is interpreted as a transfer function between the n components of the model output $\hat{y}_i$ and the plant output y_i. For coupled systems, the closed-loop interactions can be decoupled using a partial cross-spectral density analysis (Yerramilli and Tangirala, 2016).

5.2 Partial cross-spectral density

The partial cross-spectral density (PCSD) is the frequency domain analogue of the partial covariance function and is used to calculate the cross-spectral density between two datasets after the effects of a third dataset are removed (Priestley, 1981).

To obtain the PCSD between x and y, given z, first obtain the two conditioned signals,

$$\psi_{x|z}(t) = x(t) - \sum_{k=-\infty}^{\infty} b_1(k) z(t-k) \tag{13a}$$

$$\psi_{y|z}(t) = y(t) - \sum_{k=-\infty}^{\infty} b_2(k) z(t-k) \tag{13b}$$

where $b_1(k)$ and $b_2(k)$ are determined by minimizing the expectation operator $E[\psi^2_{x|z}(t)]$ and $E[\psi^2_{y|z}(t)]$ respectively. The frequency-domain representation of the conditioned signals in (13) are

$$\Psi_{x|z}(\omega) = X(\omega) - B_1(\omega) Z(\omega) \tag{14a}$$

$$\Psi_{y|z}(\omega) = Y(\omega) - B_2(\omega) Z(\omega) \tag{14b}$$

The transfer functions for b_1 and b_2 are

$$B_1(\omega) = \sum_{k=-\infty}^{\infty} b_1(k) e^{-j\omega k} = \frac{\gamma_{x,z}(\omega)}{\gamma_{z,z}(\omega)} \tag{15a}$$

$$B_2(\omega) = \sum_{k=-\infty}^{\infty} b_2(k) e^{-j\omega k} = \frac{\gamma_{y,z}(\omega)}{\gamma_{z,z}(\omega)} \tag{15b}$$

PCSD is found by evaluating the CSD between $\Psi_{x|z}$ and $\Psi_{y|z}$. Thus, the PCSD between x and y given z can be defined as,

$$\begin{aligned} \gamma_{x,y|z}(\omega) =& \gamma_{x,y}(\omega) - B_1(\omega)\gamma_{z,y}(\omega) - B_2^*(\omega)\gamma_{x,z}(\omega) \\ &+ B_1(\omega)B_2^*(\omega)\gamma_{z,z}(\omega) \\ =& \gamma_{x,y}(\omega) - \frac{\gamma_{x,z}(\omega)\gamma_{z,y}(\omega)}{\gamma_{z,z}(\omega)} \end{aligned} \tag{16}$$

where B_2^* is the complex conjugate of B_2.

5.3 Decoupled PMR for MIMO systems

Using operational data, along with the PCSD, a decoupled estimation of the PMR matrix in (11) can be derived. From (10) it is clear that for an $n \times n$ system, the confounding variables between a specific plant output and the corresponding model output are the residual $(n-1)$ contributions to the model output of the same row in the transfer function matrix. The PCSD then allows for the estimation of the decoupled PMR by removing the effects of the confounding variables for a specific component in the PMR matrix,

$$\hat{\mathbf{\Pi}}_{\boldsymbol{G},ij}(\omega) = \frac{\hat{\gamma}_{y_i,\hat{y}_{ij}|\mathbf{Z}}(\omega)}{\hat{\gamma}_{\hat{y}_{ij},\hat{y}_{ij}|\mathbf{Z}}(\omega)} \tag{17}$$

where $\mathbf{Z} = \{\hat{y}_{ik} | k \in (1, ...n), k \neq j\}$.

The decoupled PMR for an $n \times n$ system, equates to n^2 SISO systems. Each decoupled SISO sub-system is characterized by a unique input-output relationship. Thus, the SISO analysis and systematic test of Table 2 can be applied to each entry of the PMR matrix. Two items should be taken note of:

(1) Since PMR is fundamentally based on a frequency analysis, sufficient broadband excitation is required at the set-point. A single frequency sine wave will propagate only a single frequency through the system which will lead to a lack of information over a band of frequencies in the PCSD (Priestley, 1981).
(2) If the model used to describe the system is not a devitation variable model, as seen in (2a), where all operations of the system is centred about zero, the operating point of each variable within the system should be subtracted from the recorded data. Eliminating the offset in data will remove the corresponding higher frequency components that overpower the CSD and ensure accurate results for the PMR.

6. MODEL-PLANT MISMATCH DETECTION APPLIED TO THE GRINDING MILL CIRCUIT

MPC, as described in Section 2, was used to control the grinding mill circuit as represented by the model in (2). The upper and lower constraints listed in Table 1 were used along with a prediction horizon of $N_P = 20$ and a control horizon of $N_C = 5$.

The model uncertainties as described by Craig and MacLeod (1995) were used to introduce MPM into the simulation environment. In general milling circuits are nonlinear and time-varying systems. When a linearised representation for the milling circuit is used, the nonlinear and time varying characteristics of the milling circuit can be accounted for in the uncertainty description accompanying the linear model.

After finite-dimensional and linear time-invariant models were fitted to real world recorded data, the standard deviation of each model parameter was,

$$k_{ij} : \begin{bmatrix} 31\% & 14\% & 31\% \\ 65\% & 11\% & 16\% \\ - & - & - \end{bmatrix} \tag{18a}$$

$$\tau_{ij} : \begin{bmatrix} 18\% & - & 19\% \\ 40\% & - & 60\% \\ - & - & - \end{bmatrix} \tag{18b} \qquad \theta_{ij} : \begin{bmatrix} 27\% & - & - \\ - & - & - \\ - & - & - \end{bmatrix} \tag{18c}$$

This standard deviation of each model parameter indicates the amount of change or uncertainty that can be expected

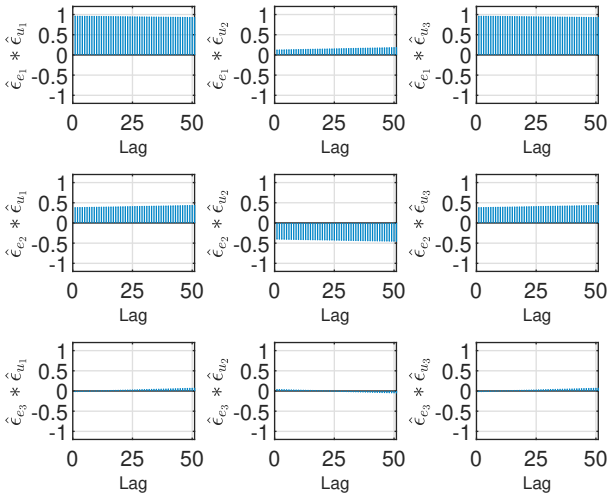

Fig. 3. Cross correlation between $\hat{\epsilon}_{e_j}$ and $\hat{\epsilon}_{u_i}$

and therefore these real world indicators are used as the model uncertainty description. The dashes indicate that the relative uncertainty of the particular parameter is insignificant. For the simulations in Section 6.1 and Section 6.2 the first row of (18a) and (18b) will be applied as an overestimation, for example $k_{11_{plant}} = k_{11} \times (1 + 31\%)$, while the second row of (18a) and (18b) will be applied as an underestimation, for example $k_{21_{plant}} = k_{21} \times (1 - 65\%)$. The single delay uncertainty in (18c), will be applied as an overestimation $\big(\theta_{11_{plant}} = \theta_{11} \times (1 + 27\%)\big)$. These selections were made to evaluate if PMR can identify the direction of MPM.

As noted in Section 4 and Section 5, the main difference in MV excitation between the two MPM detection techniques is that the partial correlating analyses requires at least a single large step for sufficient MV excitation. For PMR, a broadband excitation is required in the form of a set of small steps. These different excitation requirements are considered during the simulations.

6.1 Partial Correlation Analyses

For the partial correlation analyses simulations, the set-point of y_{J_T} was changed from 45% to 50% to ensure sufficient MV excitation. For the simulation results, the partial correlation between $\hat{\epsilon}_{e_j}$ and $\hat{\epsilon}_{u_i}$ at lags of 0 to 50 is depicted in Fig. 3. Using an empirical threshold of 0.01 to differentiate between zero and nonzero correlations, it is evident that only g_{31}, g_{32} and g_{33} can be classified with no MPM. The average partial cross correlation can be seen in Table 3 and it is evident that the correct MPM is identified based on (18).

6.2 Plant Model Ratio

For PMR simulations, a normally distributed white noise signal, with signal power of 0.01, is added to each set-point to ensure sufficient broadband frequency excitation. The systematic test for MPM detection using PMR, from Table 2, is applied to the estimated magnitude spectra in Fig. 5 and the estimated phase spectra in Fig. 4. For step 1 in the summarized results (Table 4), it is evident that $M_{1j}(0) > 1$ while $M_{2j}(0) < 1$ and $M_{3j}(0) = 1$, confirming the gain mismatch estimation error as described in (18a). From Fig. 5, the initial gradient of the estimated magnitude spectra, plotted in orange, confirm the overestimation in plant dynamics for g_{11} and g_{13} with an initial positive gradient in $M_{11}(\omega)$ and $M_{13}(\omega)$ while also confirming the underestimation of plant dynamics in g_{21} and g_{23} with and initial negative gradient in $M_{21}(\omega)$ and $M_{23}(\omega)$. The overestimation of the delay in g_{11} can be seen in the estimated phase spectra (Fig. 4) with a positive gradient in ΔP_{11} (plotted in orange).

These simulations correctly isolated and diagnosed the MPM as described using the model uncertainties in (18), providing a suitable alternative to MPM analysis, with the option of identifying the type and direction of mismatch within a specific input-output channel, for a grinding mill circuit.

Table 3. Average partial cross correlation results

	$\hat{\epsilon}_{\mathbf{u_1}}$	$\hat{\epsilon}_{\mathbf{u_2}}$	$\hat{\epsilon}_{\mathbf{u_3}}$
$\hat{\epsilon}_{\mathbf{e_1}}$	0.940	0.149	0.940
$\hat{\epsilon}_{\mathbf{e_2}}$	0.404	-0.424	0.406
$\hat{\epsilon}_{\mathbf{e_3}}$	0.026	-0.005	0.026

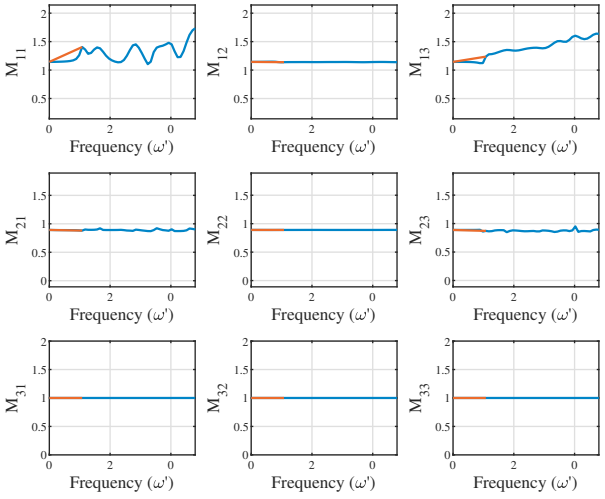

Fig. 4. Estimated PMR magnitude spectra.

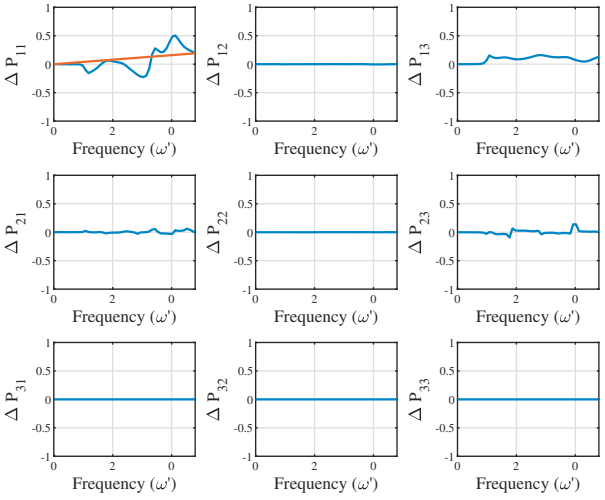

Fig. 5. Estimated PMR phase spectra.

Table 4. PMR Results

		Π_{i1}	Π_{i2}	Π_{i3}
Step 1 $M_{ij}(0)$	Π_{1j}	1.143	1.144	1.144
	Π_{2j}	0.892	0.890	0.888
	Π_{3j}	1	1	1
Step 2 $M(\omega)$ **initial slope**	Π_{1j}	0.968	-0.008	0.343
	Π_{2j}	-0.042	-5.163×10^{-4}	-0.063
	Π_{3j}	0	0	0
Step 3 ΔP	Π_{1j}	0.159	1.539×10^{-4}	0.020
	Π_{2j}	-0.003	-2.986×10^{-4}	-7.254×10^{-4}
	Π_{3j}	0	0	0

7. CONCLUSION

The two methods of MPM identification, as described in Section 4 and Section 5, are tested on the grinding mill circuit as described in Section 3. The results for the correlation-based method, shown in Section 6.1 matched the previous work of Olivier and Craig (2011) in that MPM in a specific transfer function of a MIMO LTI system can correctly be identified. The transfer function that contains the MPM can then be re-identified using suitable system identification techniques. One of the disadvantages of this MPM methodology is that large set-point step changes are necessary for sufficient MV excitation.

From the results in Section 6.2, it is evident that PMR as an improved MPM identification technique yields better results than the partial correlation analyses when applied to the milling circuit. The specific transfer function identification is identical in the sense that the input-output channel can be identified in both cases. Howerver, the added benefits of using the PMR is that the type and direction of mismatch for an LTI system can be identified with a relatively nonbelligerent white noise signal added to the set-point.

Future work includes the investigation on shaping the noise signal imposed on the set-points to allow for specific frequencies to be excluded from the PMR analyses. The shaping of the dithering signal will also aid in minimizing the strenuous effects that a rapidly changing discrete white noise signal will have on the milling circuit actuators. This may prolong the life expectancy of the milling circuit equipment.

REFERENCES

Badwe, A.S., Gudi, R.D., Patwardhan, R.S., Shah, S.L., and Patwardhan, S.C. (2009). Detection of model-plant mismatch in MPC applications. *J. Process Contr.*, 19(8), 1305–1313.

Coetzee, L.C., Craig, I.K., and Kerrigan, E.C. (2010). Robust nonlinear model predictive control of a run-of-mine ore milling circuit. *IEEE T. Contr. Syst. T.*, 18(1), 222–229.

Craig, I.K. and MacLeod, I.M. (1995). Specification framework for robust control of a run-of-mine ore milling circuit. *Control Eng. Pract.*, 3(5), 621–630.

Hodouin, D. (2011). Methods for automatic control, observation, and optimization in mineral processing plants. *J. Process Contr.*, 21(2), 211–225.

Jiang, H., Huang, B., and Shah, S.L. (2009). Closed-loop model validation based on the two-model divergence method. *J. Process Contr.*, 19(4), 644–655.

Kaw, S., Tangirala, A.K., and Karimi, A. (2014). Improved methodology and set-point design for diagnosis of model-plant mismatch in control loops using plant-model ratio. *J. Process Contr.*, 24(11), 1720–1732.

le Roux, J.D. and Craig, I.K. (2019). Plant-Wide Control Framework for a Grinding Mill Circuit. *Ind. Eng. Chem. Res.*, 58(26), 11585–11600.

Li, L., Lu, L., Huang, Z., Chen, X., and Yang, S. (2020). A model mismatch assessment method of MPC by decussation. *ISA T.*, 106, 51–60.

Ling, D., Zheng, Y., Zhang, H., Yang, W., and Tao, B. (2017). Detection of model-plant mismatch in closed-loop control system. *J. Process Contr.*, 57, 66–79.

Mayne, D.Q. (2014). Model predictive control: Recent developments and future promise. *Automatica*, 50(12), 2967–2986.

Olivier, L.E. and Craig, I.K. (2011). Parameter mismatch detection in a run-of-mine ore milling circuit under Model Predictive Control. *IFAC PapersOnLine*, 44(1), 9929–9934.

Olivier, L.E. and Craig, I.K. (2017). A survey on the degree of automation in the mineral processing industry. In *2017 IEEE AFRICON*, 404–409.

Priestley, M.B. (1981). *Spectral Analysis and Time Series*. Academic Press, London ; New York.

Qin, S. and Badgwell, T.A. (2003). A survey of industrial model predictive control technology. *Control Eng. Pract.*, 11(7), 733–764.

Schwenzer, M., Ay, M., Bergs, T., and Abel, D. (2021). Review on model predictive control: An engineering perspective. *Int. J. Adv. Manuf. Technol.*, 117(5), 1327–1349.

Selvanathan, S. and Tangirala, A.K. (2010). Diagnosis of poor control loop performance due to model-plant mismatch. *Ind. Eng. Chem. Res.*, 49(9), 4210–4229.

Tsai, Y., Gopaluni, R.B., Marshman, D., and Chmelyk, T. (2015). A novel algorithm for model-plant mismatch detection for model predictive controllers. *IFAC PapersOnLine*, 48(8), 746–752.

Wei, D. and Craig, I.K. (2009). Grinding mill circuits — A survey of control and economic concerns. *Int. J. Miner. Process*, 90(1-4), 56–66.

Wu, Q. and Du, W. (2022). Online detection of model-plant mismatch in closed-loop systems with Gaussian processes. *IEEE T. Ind. Inform.*, 18(4), 2213–2222.

Xu, X., Simkoff, J.M., Baldea, M., Chiang, L.H., Castillo, I., Bindlish, R., and Ashcraft, B. (2020). Data-driven plant-model mismatch estimation for dynamic matrix control systems. *Int. J. Robust Nonlin.*, 30(17), 7103–7129.

Yerramilli, S. and Tangirala, A.K. (2016). Detection and diagnosis of model-plant mismatch in MIMO systems using plant-model ratio. *IFAC PapersOnLine*, 49(1), 266–271.

Yin, F., Wang, H., Xie, L., Wu, P., and Song, Z. (2014). Data driven model mismatch detection based on statistical band of Markov parameters. *Comput. Electr. Eng.*, 40(7), 2178–2192.